HHS Public Access

Author manuscript

DNA Repair (Amst). Author manuscript; available in PMC 2024 March 01.

Published in final edited form as:

DNA Repair (Amst). 2023 March ; 123: 103452. doi:10.1016/j.dnarep.2023.103452.

Polβ/XRCC1 heterodimerization dictates DNA damage recognition and basal Polβ protein levels without interfering with mouse viability or fertility

Christopher A. Koczor[1,2], **Marlo K. Thompson**[1,3,#], **Nidhi Sharma**[1,3,#], **Aishwarya Prakash**[1,3,*], **Robert W. Sobol**[1,2,4,*]

[1]Mitchell Cancer Institute, University of South Alabama, Mobile, AL 36604, USA

[2]Department of Pharmacology, College of Medicine, University of South Alabama, Mobile, AL 36688, USA

[3]Department of Biochemistry and Molecular Biology, College of Medicine, University of South Alabama, Mobile, AL 36688, USA

[4]Department of Pathology and Laboratory Medicine, Warren Alpert Medical School & Legorreta Cancer Center, Brown University, Providence, RI 02912

Abstract

DNA Polymerase β (Polβ) performs two critical enzymatic steps during base excision repair (BER) - gap filling (nucleotidyl transferase activity) and gap tailoring (dRP lyase activity). X-ray repair cross complementing 1 (XRCC1) facilitates the recruitment of Polβ to sites of DNA damage through an evolutionarily conserved Polβ/XRCC1 interaction interface, the V303 loop. While previous work describes the importance of the Polβ/XRCC1 interaction for human Polβ protein stability and recruitment to sites of DNA damage, the impact of disrupting the Polβ/XRCC1 interface on animal viability, physiology, and fertility is unknown. Here, we characterized the effect of disrupting Polβ/XRCC1 heterodimerization in mice and mouse cells by complimentary approaches. First, we demonstrate, via laser micro-irradiation, that mouse Polβ amino acid

[*]**Address correspondence to**: Robert W. Sobol, Ph.D., Department of Pathology and Laboratory Medicine, Warren Alpert Medical School, Legorreta Cancer Center, Brown University, Providence, RI 02912, rwsobol@brown.edu, Aishwarya Prakash, Ph.D., University of South Alabama, Department of Biochemistry and Molecular Biology, Mitchell Cancer Institute, 1660 Springhill Avenue, Mobile, AL 36604, aprakash@southalabama.edu.

[#]These authors contributed equally to this work.

CRediT authorship contribution statement

Christopher A. Koczor: Conceptualization, Data curation, Investigation, Methodology, Writing - original draft, Writing - review & editing, Marlo K. Thompson: Data curation, Investigation, Methodology, Writing - review & editing, Nidhi Sharma: Data curation, Investigation, Methodology, Writing - review & editing, Aishwarya Prakash: Conceptualization, Funding acquisition, Project administration, Supervision, Writing - original draft, Writing - review & editing, Robert W. Sobol: Conceptualization, Funding acquisition, Project administration, Supervision, Writing - original draft, Writing - review & editing.

Declaration of Competing Interest

RWS is a scientific consultant for Canal House Biosciences, LLC. The authors state that there is no conflict of interest.

Supplementary Data

Supplementary material related to this article can be found, in the online version, at doi:10.1016/j.dnarep.2023.103452

residues L301 and V303 are critical to facilitating Polβ recruitment to sites of DNA damage. Next, we solved the crystal structures of mouse wild type Polβ and a mutant protein harboring alterations in residues L301 and V303 (L301R/V303R). Our structural analyses suggest that Polβ amino acid residue V303 plays a role in maintaining an interaction with the oxidized form of XRCC1. Finally, we created CRISPR/Cas9-modified *Polb* mice with homozygous L301R/V303R mutations ($Polb^{L301R\text{-}V303R/L301R\text{-}V303R}$) that are fertile yet exhibit 15% reduced body weight at 17 weeks of age, as compared to heterozygous mice. Fibroblasts derived from $Polb^{L301R\text{-}V303R/L301R\text{-}V303R}$ mice demonstrate that mutation of mouse Polβ's XRCC1 interaction domain leads to an ~85% decrease in Polβ protein levels. In all, these studies are consistent with a role for the oxidized form of XRCC1 in providing stability to the Polβ protein through Polβ/XRCC1 heterodimer formation.

Graphical Abstract

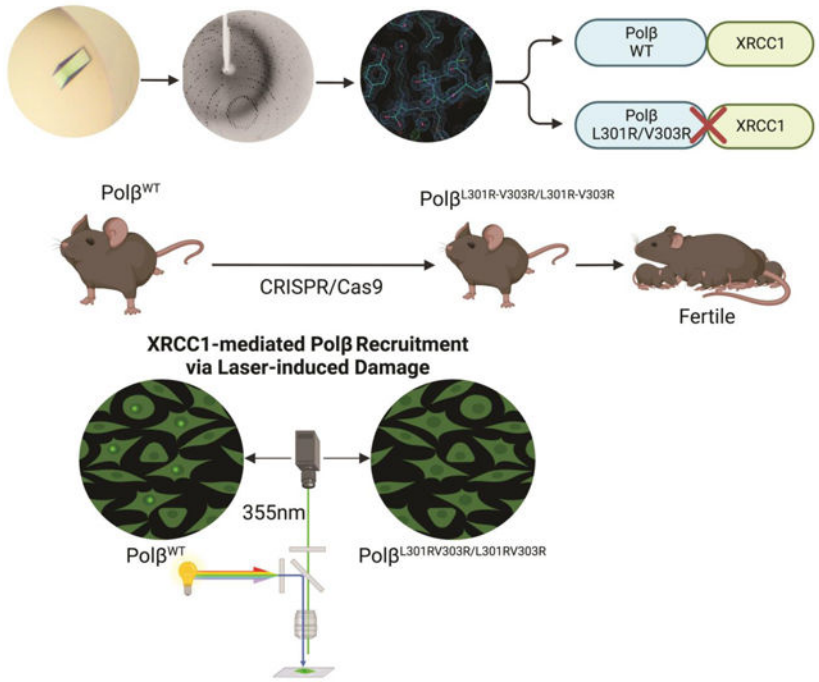

Keywords

DNA Polymerase beta; XRCC1; protein interactions; X-ray crystallography; mouse model

1. Introduction

Base excision repair (BER) is an evolutionarily conserved DNA repair pathway that is essential for the repair and resolution of approximately 20,000 base lesions per cell per day in both the nuclear and mitochondrial genomes [1, 2]. BER and single-strand break repair (SSBR) mechanisms facilitate repair of base damage and DNA single-strand breaks [3, 4]. This repair process helps avoid the accumulation of genome destabilizing base damage and BER intermediates which contribute to genomic instability, increased genetic mutations

(base alterations, strand breaks), cancer development, and cancer progression [5, 6]. BER is a multiple step pathway defined by lesion recognition and incision (i.e., via a DNA glycosylase and APE1/PNKP), DNA gap tailoring (by DNA polymerase β, Polβ), and DNA synthesis and ligation (by Polβ and DNA ligases I and III) [7].

Polβ catalyzes two separate and essential enzymatic functions utilized during BER (5'dRP lyase for gap tailoring, and nucleotidyl transferase for DNA synthesis), and *Polb* knockout mice do not survive long after birth, highlighting its cellular importance [8–11]. To facilitate lesion access and the rapid formation of BER protein complexes in chromatinized DNA, these reaction steps are coordinated following poly(ADP-ribose) (PAR) polymerase 1 (PARP1) and PARP2 activation and production of poly(ADP-ribose) (PAR) [12]. The subsequent formation of BER protein complexes are then assembled via the PAR-binding scaffold protein X-ray repair cross complementing 1 (XRCC1) [13, 14]. Through its PAR binding domain (PBD), XRCC1 binds to PAR and facilitates the recruitment of BER/SSBR factors including Polβ, APTX and DNA ligase III to sites of DNA damage. Importantly, the recruitment of Polβ is dependent on the interaction with XRCC1 via a defined protein-protein interaction domain [12, 15, 16].

We previously reported that disruption of the human Polβ/XRCC1 interaction led to diminished Polβ protein abundance [17]. Given the importance of Polβ on mouse survival, we herein investigated the role of the Polβ/XRCC1 interaction in a mouse model with targeted mutations in Polβ at the Polβ/XRCC1 interaction interface. We demonstrate that evolutionarily conserved Polβ amino acid residues L301 and V303 play a crucial role in mediating the Polβ/XRCC1 interaction in the mouse and in mouse cells. Disruption of L301 or V303 through a single mutation significantly reduces mouse Polβ protein recruitment to sites of DNA damage, while the dual mutation (Polβ L301R/V303R) does not bind XRCC1 and causes no detectable protein recruitment to sites of laser-induced DNA damage.

Numerous structures of human Polβ have been solved via X-ray crystallography [18–21]. Here, for the first time, we studied the unliganded crystal structures of truncated wild-type (WT) mouse Polβ and the Polβ L301R/V303R dual mutation, each lacking the N-terminal 8 kDa lyase domain. Superposition of our mouse Polβ mutant model with the structure of rat Polβ protein complexed with the oxidized form of human XRCC1 [22] reveals that mutation of V303 to arginine would cause a direct clash with proline 2 of XRCC1, thereby leading to the likely destabilization of the Polβ/XRCC1 complex. Further, we generated CRISPR/Cas9-mediated Polβ L301R/V303R mice ($Polb^{WT/L301R\text{-}V303R}$) and successfully bred them to homozygosity, suggesting loss of the Polβ/XRCC1 interaction is not necessary for survival, development, or fertility. Although the $Polb^{L301R\text{-}V303R/L301R\text{-}V303R}$ mice were smaller in size, they did not display any behavioral or stress-associated phenotypes, to-date. Finally, we verified that fibroblasts generated from $Polb^{L301R\text{-}V303R/L301R\text{-}V303R}$ mice do not show sensitivity to genotoxic stress but demonstrate significantly lower Polβ protein abundance similar to studies with human cells [17, 23].

2. Materials and Methods

2.1 Reagents and chemicals

All plasmids, antibodies, chemicals, and other resources and reagents used in this study are listed in Table S1. The EGFP-Polβ lentiviral vectors were designed in-house and then purchased from VectorBuilder (Chicago, IL). The pGEX-4T3-mPOLB(WT) and pGEX-4T3-mPOLB(L301R/V303R) expression vectors were designed in-house and then purchased from GenScript USA (Piscataway, NJ).

2.2 Cells and cell culture

The SV40 Large T-antigen immortalized *Polb*(−/−) mouse embryonic fibroblast cell line 88TAg was created as previously described [10, 24]. The 88TAg cells are available from ATCC (Cat# CRL-2820), Kerafast (Cat# ENH116-FP), and ABMGood (Cat# T3170). 88TAg cells were cultured in DMEM supplemented with 10% heat-inactivated fetal bovine serum, 1% Glutamax, and 1% penicillin/streptomycin and maintained in tissue culture incubators at 37°C, 5% CO_2.

For generation of immortalized mouse ear fibroblast cells, tissue from the ears of $Polb^{L301R\text{-}V303R/L301R\text{-}V303R}$ or littermate WT mice were processed as previously described [25]. Briefly, mice were euthanized by CO_2 and cervical dislocation, and tissue from the ears were harvested and processed independently for each line. Ears were briefly washed in 70% ethanol before being cut into small pieces (~3mm) and digested with collagenase and the Pronase protease for 1.5 hours at 37°C with continuous shaking. Enzymatically digested tissues were ground and filtered through a 70μm cell strainer, centrifuged twice at 580xg for 7 min, then plated into 100mm dishes for growth. Cells were cultured in RPMI 1640 media supplemented with 10% heat-inactivated fetal bovine serum, asparagine (100μM), 2-mercaptoethanol (50μM), 2mM glutamine, 1% antibiotic/antimycotic, and 1% penicillin/streptomycin. Amphotericin B (1:1000) was added to the media for the first 2 weeks that cultures were being established. After 1 week and following 2 cell passages, the remaining fibroblasts were immortalized by transfection with an SV40 T-antigen encoded plasmid (pSVAgT), as we described previously [24]. Cells were passaged twice after SV40 T-antigen immortalization prior to experimentation.

2.2 Lentivirus production and cell transduction

Lentiviral particles were generated by co-transfection of 4 plasmids into 293-FT cells using TransIT-X2 Transfection reagent: the packaging vectors pMD2.g(VSVG), pVSV-REV, and pMDLg/pRRE together with the appropriate shuttle vectors. Forty-eight (48) hrs after transfection, lentivirus-containing supernatant was collected and passed through 0.45μm filters to isolate the viral particles as described previously [17, 26].

Lentiviral transduction was performed as follows: 88TAg cells (1×10^5) were seeded into 6-well plates. Twenty-four (24) hrs later, lentiviral particles (1ml) were mixed with polybrene (2μg/ml) and added to the cells. Cells were incubated at 32°C overnight, and then medium with lentiviral particles was replaced with fresh medium. For transient expression

experiments, cells were then cultured for at least 96 hrs, but no more than two weeks, at 37°C, before experimental analysis.

2.3 Laser micro-irradiation

For laser micro-irradiation, 5×10^4 cells were seeded into each well of an 8-chamber glass bottom vessel (Thermo Fisher Scientific, #155409). Twenty-four (24) hrs later, laser micro-irradiation and subsequent time-lapse imaging were performed using a Nikon A1rsi laser scanning confocal microscope equipped with 6 visible wavelength lasers (405, 441, 514, 561, 647nm, Coherent), customized to add a UVA 355nm laser (PicoQuant) controlled by a Bruker XY Galvanometer, and equipped with a live-cell incubation chamber (Tokai Hit) maintained at 5% CO_2 and 37°C, using a 40x (NA=1.4) oil-immersion objective for 355nm laser micro-irradiation. For parallel irradiation, time lapse images were collected every 15 s during a 10 min interval. Images of focal recruitment were quantified using the MIDAS software package for quantitation and statistical analysis of focal recruitment [12]. At least forty individual cells (2 sets of 10 cells were performed on 2 separate days) were analyzed and used to generate recruitment profiles and kinetic parameters.

2.4 Cell protein extract preparation and immunoblot

Cells were seeded into a 60mm cell culture dish. After reaching 75–80% confluency, cells were washed twice with cold PBS, collected, and lysed with an appropriate volume of 2x clear Laemmli buffer (2% SDS, 20% glycerol, 62.5mmol/l Tris-HCl pH 6.8). Cell lysates were boiled for 10 min and quantified with the DC protein assay kit following the microplate protocol provided by the company (Bio-Rad).

Whole cell protein lysates (15–40μg protein) were loaded onto precast NuPAGE 412% Bis-Tris gels and run for 1 hr at 120V. Gel electrophoresis separated proteins were transferred onto a PVDF membrane using a Turboblotter (Bio-Rad). The membrane was first blocked with B-TBST (TBS buffer with 0.05% Tween-20 and supplemented with 5% blotting grade non-fat dry milk; Bio-Rad) for 1 hr at room temperature and subsequently blotted with the primary antibodies in B-TBST overnight at 4°C. The primary antibodies and their dilutions are listed in Table S1. After washing, membranes were incubated with secondary antibodies in B-TBST for 1 hr (room temperature). The following HRP conjugated secondary antibodies were used: Bio-Rad Goat anti-mouse-HRP conjugate and Bio-Rad anti-rabbit-HRP conjugate (see Table S1). After washing, the membrane was illuminated with a chemiluminescent substrate. Protein bands were imaged using a Bio-Rad Chemi-Doc MP imaging system.

2.5 EGFP-Polβ/XRCC1 immunoprecipitation

88TAg mouse embryonic fibroblast (MEF) cells were transduced with lentivirus encoding EGFP-Polβ or the indicated EGFP-Polβ mutants. Cells were expanded using two 150mm dishes for each cell line, at which point the cells were lysed and EGFP-Polβ was immunoprecipitated using a GFP-Trap kit (Chromotek), following the manufacturer protocols. Cells were lysed (10mM Tris/HCl pH 7.5, 150mM NaCl, 0.5mM EDTA, 0.5% Nonidet P40) at 4°C for 30 minutes followed by centrifugation for 10 min at 14,000rpm and 4°C to clear the lysate of cellular debris. Samples were then diluted with dilution buffer

(10mM Tris/HCl pH 7.5, 150mM NaCl, 0.5mM EDTA) and then added to pre-equilibrated GFP-Trap magnetic beads to capture EGFP-Polβ and the bound proteins. Beads and protein were incubated at 4°C for 60 min with continuous inversion. Beads were then washed three times with wash buffer (10mM Tris/HCl pH 7.5, 150mM NaCl, 0.5mM EDTA, 0.05% Nonidet P40). Proteins were eluted from the beads by boiling for 10 min and loaded onto SDS-PAGE gels for immunodetection of Polβ and XRCC1. Immunoblot bands were quantified, with XRCC1 band density normalized to Polβ band density. Experiments were performed at least twice for lysates from cells expressing each EGFP-Polβ vector.

2.6 Polβ protein expression and purification

The pGEX4T3 expression vectors encoding full length (amino acids residues 1–335) or truncated (i.e., amino acids residues 88–335) WT and mutant (L301R/V303R) mouse Polβ were used to express the proteins in Rosetta 2(DE3)pLysS cells (Novagen) following induction by 1mM IPTG at 37°C for 2.5 hours. Cells were lysed in a buffer containing 50mM HEPES pH 7.4, 500mM NaCl, 1mM ethylenediaminetetraacetic acid (EDTA), and 1mM dithiothreitol (DTT) in the presence of 1mM phenylmethylsulfonyl fluoride (PMSF) and 1× complete EDTA-free protease inhibitor cocktail (Roche). Crude clarified lysate was incubated with glutathione sepharose beads (Cytiva) for 2 hours. The resin was washed with buffer A (50mM HEPES pH 7.4, 100mM NaCl, and 1mM DTT) and resuspended for cleavage of the GST tag by addition of 0.5mg purified TEV protease per 5mL of resuspended resin. The protein elutes in the flow through and is subsequently subjected to ion exchange chromatography in buffer A followed by a gradient elution with 1M NaCl. Protein preparations were concentrated to 10–20mg/ml and flash cooled in liquid nitrogen for long-term storage.

2.7 Protein crystallization and data collection

Crystallization drops were prepared by mixing 0.5μL protein (5mg/mL WT and 7.9mg/mL mutant) and 0.5μL reservoir solution containing 0.1M HEPES pH 7.5, 22.5–27.5% w/v PEG 3350, and 1.5% v/v tacsimate pH 7.0. Crystals were obtained between 6–27 days, mounted onto MiTeGen micro-loops, cryoprotected (0.1M HEPES pH 7.5, 22.5% w/v PEG 3350, 1.5% v/v tacsimate pH 7.0, and 14% v/v ethylene glycol), and flash cooled in liquid nitrogen. X-ray diffraction data were collected on a Home Source (D8 Quest, Bruker). Data (20 sec per exposure) were collected to 1.65Å for the WT with a crystal-to-detector distance of 75mm and an image width of 0.2° per frame. For the mutant (L301R/V303R), data (20 sec per exposure) were collected to 1.8Å with a crystal-to-detector distance of 60mm and an image width of 0.2° per frame.

2.8 Structure determination and refinement

The structures of mPolβ WT and mutant (L301R/V303R) were obtained by Molecular Replacement using Phaser-MR within the PHENIX suite using the WT rat Polβ model (PDB code 1ZQY) [27, 28]. A preliminary model of the WT and mutant (L301R/V303R) truncated mPolβ were achieved from molecular replacement solution with translational function Z-scores of 15.8 and 11.9, respectively. Models were built using Coot and refined using Phenix with >99% of residues in the preferred Ramachandran regions as determined by MolProbity [29, 30]. Coordinates were deposited to the protein data bank (PDB) with the

codes 8E10 and 8E11 for the WT and mutant structures, respectively. All superimpositions, RMSD values, and structural figures were generated with MacPyMOL (The PyMOL Molecular Graphics System, Version 1.7.6.2; Schrödinger, LLC).

2.9 Polb$^{WT/L301R-V303R}$ mouse generation

The *Polb*$^{WT/L301R-V303R}$ mouse was generated by the University of Alabama Birmingham (UAB) Transgenic and Genetically Engineered Models (TGEM) Core. Two CRISPR guide RNAs (G1: 5'- GTACACCATCCGCCCCCTGG-3'; G2: 5'-ATCCGCCCCCTGGGGGTCAC-3') were designed using CRISPOR.tefor.net to target exon 13 of the mouse *Polb* locus. Two symmetrical 100bp ssDNA repair templates were designed to introduce variants L301R and V303R, subsequently eliminating an XcmI restriction site that could be used for genotyping. The CRISPR guide and Cas9 protein were complexed *in vitro* before injection at a concentration of 50ng/μl of each guide RNA, 50ng/μl Cas9 protein, and 50ng/μl ssDNA repair template into 0.5-day old C57Bl/6 mouse embryos. Embryos surviving microinjection were transferred into pseudo-pregnant recipients to develop to term. PCR amplification of genomic DNA extracted from pup tail biopsy at weaning and XcmI restriction digestion of the PCR amplicon were used to verify on target CRISPR activity. Sanger sequencing of the cloned PCR products confirmed correct integration of the intended variants. Upon receipt from UAB, the *Polb*$^{WT/L301R-V303R}$ mice were bred to C57/Bl6 mice (Jackson Labs) and then *Polb*$^{WT/L301R-V303R}$ mice from different litters were interbred to generate a homozygous colony (*Polb*$^{L301R-V303R/L301R-V303R}$). All animal breeding was performed according to the institutional guidelines at the University of South Alabama (IACUC Protocol # 1577899–3).

2.10 Genotoxicity analysis

Polb$^{L301R-V303R/L301R-V303R}$ mouse ear fibroblasts were plated into a 96-well dish at a density of 1×10^4 cells per well, with 6 wells per cell line assayed. Cells were treated with methyl methanesulfonate (MMS) or hydrogen peroxide (H_2O_2) at the concentrations noted, and cells were allowed to grow for 5 days. After 5 days, cells were fixed using 4% paraformaldehyde containing 20μM Hoechst 33342 dye. Cell nuclei were imaged and counted using a Celigo S Imaging Cytometer (Nexcelom Bioscience) and analyzed using GraphPad Prism (V9).

2.11 Statistical analysis

Averages and standard error of the mean (SEM) were calculated from the means (on technical replicates) of multiple independent experiments (n = number of independent experiments as indicated in figure legends), unless stated otherwise. Student's t-test or ANOVA (with a Tukey *post-hoc* test) was used to test for significant differences as appropriate, with results generally compared to controls and as indicated in the figure legends. In cases where comparisons are made to a different experimental group besides the control, it is stated in the figure legend. P-values are indicated by asterisks (*$p<0.05$, **$p<0.01$, ***$p<0.001$, ****$p<0.0001$) or are stated in the figure legend. Statistical analyses were performed using GraphPad Prism except those explicitly determined in MIDAS.

3. Results

3.1 Mutation of mouse Polβ amino acid residues L301/V303 (L301R/V303R) disrupts Polβ/XRCC1 complex formation

Polβ maintains a genetically conserved XRCC1 interaction domain in the C-terminus [22] (Figs. 1A, S1A). Previous research by our group and others have identified Polβ amino acid residues L301, V303, and V306 as facilitating the interaction with XRCC1 [17, 31], but these studies focused primarily on the human protein (Polβ/XRCC1) complex. We recently demonstrated that the recruitment of human Polβ to sites of laser-induced DNA damage is dependent on its interaction with XRCC1 [12], confirming the role of the Polβ/XRCC1 interaction domain (the V303 loop) on BER protein complex assembly. To determine if Polβ amino acid residues L301, V303, and V306 similarly facilitate the Polβ/XRCC1 interaction in mouse cells, we expressed an EGFP-fusion of the WT mouse protein (EGFP-Polβ) or those with individual mutations or combination mutations in Polβ knockout MEF cells (88TAg) and subsequently laser micro-irradiated the cells to induce DNA damage, as previously described [12]. Individual mutations in the V303 loop of EGFP-Polβ (L301R, V303R, and V306R) significantly reduced laser-induced focal recruitment, as compared to EGFP-Polβ (Figs. 1B,C and S1B). Peak recruitment intensity was diminished in EGFP-Polβ L301R, V303R, and V306R; decreased by 58.3%, 90.8%, and 82.6%, respectively (Fig. 1D). EGFP-Polβ dual mutant L301R/V303R and the triple mutant L301R/V303R/V306R also demonstrated reduced focal recruitment, with no visibly detectable foci formed following laser micro-irradiation (Figs. 1B,C and S1B). Peak recruitment intensity was significantly diminished for EGFP-Polβ L301R/V303R and L301R/V303R/V306R (95.8% decreased for both) (Fig. 1D), though both mutants were not statistically different from non-micro-irradiated control cells. These results demonstrate that the mouse Polβ L301R/V303R dual mutant prevents XRCC1-mediated Polβ recruitment to laser-induced DNA damage to a similar degree as the Polβ L301R/V303R/V306R triple mutant. We validated these findings using EGFP-Polβ immunoprecipitation assays and quantifying XRCC1 binding. Quantification of immunoblot images showed that Polβ V303R, L301R/V303R, and L301R/V303R/V306R mutants attenuated XRCC1 binding, as compared to the WT sequence of Polβ, with complete attenuation of complexation due to the V303R mutation alone (Figs. 1E and S1C).

3.2 Structural investigations indicate that the V303R mutation likely disrupts the PolB-XRCC1^{oxo} complex

Several crystal structures of human and rat Polβ have been previously determined [18, 22, 32–34], among many other structures. Here we present the first crystal structures of mouse WT Polβ and the Polβ L301R/V303R double mutant. There is considerable sequence conservation between Polβ across species, where the protein sequence of mouse Polβ differs from that of human Polβ by 12 amino acid residues and from that of rat by only 8 residues (Fig. S1A). We obtained diffraction quality crystals of purified unliganded WT and L301R/V303R mouse Polβ lacking the N-terminal 8 kDa lyase domain (*i.e.,* amino acid residues 88–335; Fig. S2A). The crystal structures of both WT and mutant Polβ comprise two molecules each in the asymmetric unit, however mutation of L301 and V303 to arginine resulted in crystals that belonged to a different space group than the WT enzyme

(monoclinic for the mutant protein vs. orthorhombic for the WT protein; Table 1; Fig. S2B). We also note overall differences in crystal packing in the mutant Polβ L301R/V303R structure owing to the formation of a network of stabilizing salt bridge interactions between R301 and R303 and glutamate and aspartate residues from neighboring symmetry mates as depicted in Fig. S2C. Each chain of both the WT and mutant Polβ structures comprise a thumb, palm, and fingers domain where the impact of the mutations (L301R and V303R) on the overall structure appears to be minimal with an overall RMSD value of 0.536Å for all Cα atoms between the WT and mutant Polβ models (Chain A of both structures was used for the comparison; Fig. 2A). The conformation of the V303 loop did not change significantly between the WT and mutant Polβ structures with RMSD values of 0.305Å and 0.314Å for Cα and backbone atoms, respectively (Fig. 2A). We observed clear electron density for the arginine residues at positions 301 and 303 and surrounding residues in the V303 loop using a simulated annealing composite omit map contoured at 1σ (Fig. 2B).

To investigate the impact of the arginine mutations on the interaction of Polβ with XRCC1, we superimposed our L301R/V303R mutant Polβ model with the previously solved crystal structures of rat Polβ (residues 141–335) in complex with the oxidized form of human XRCC1 ($XRCC1^{oxo}$; PDB ID: 3LQC) or rat Polβ (residues 91–335) in complex with the reduced form of human XRCC1 ($XRCC1^{red}$; PDB ID: 3K75) [22]. Minor rearrangements in the side chain orientations of Polβ E309 and D321 mediate an interaction with XRCC1 residues R109 and R100 by formation of salt bridges when the binding partner is present (Fig. 3). We manually mutated rat Polβ residues L301 and V303 to arginine in the structures with the oxidized and reduced forms of XRCC1 (yellow sticks, Fig. 3) and oriented the arginine side chain based on our Polβ mutant model. Interestingly, we noted that the mutation of Polβ V303 to arginine in the $XRCC1^{oxo}$/Polβ complex results in a direct clash with P2 of $XRCC1^{oxo}$ (Fig. 3A). In the $XRCC1^{red}$/Polβ complex, P2 of XRCC1 is situated >25Å from the interaction interface due to differences in folding topology between XRCC1 in the reduced vs oxidized forms (Fig. 3B) [22]. Based on our current model, we surmise that the Polβ V303R mutation could destabilize the XRCC1/Polβ interaction depending upon the redox status of XRCC1.

3.3 Mice with the Polβ L301R/V303R mutation are viable and fertile, yet smaller in size

Previous studies found that *Polb* knockout (KO) mice died perinatally, highlighting the importance of Polβ for mouse viability [8–11]. We sought to clarify the role of Polβ's genetically conserved XRCC1 binding domain regarding mouse viability by creating a targeted germline *Polb* L301R/V303R mutation that eliminated Polβ's XRCC1 binding capacity while preserving Polβ's 5'dRP lyase and polymerase enzymatic functions. We utilized CRISPR/Cas9 to generate targeted mutations at the codons corresponding to Polβ L301/V303 on *Polb* exon 13, altering only 3 base pairs to create $Polb^{WT/L301R\text{-}V303R}$ mice (Fig. 4A). Hemizygous mice were validated by Sanger sequencing to verify both mutations were on the same allele. $Polb^{WT/L301R\text{-}V303R}$ mice were successfully bred to homozygosity ($Polb^{L301R\text{-}V303R/L301R\text{-}V303R}$), and offspring could be successfully differentiated from wild-type and $Polb^{WT/L301R\text{-}V303R}$ mice through genotyping using XcmI restriction digestion (Fig. S3A). $Polb^{L301R\text{-}V303R/L301R\text{-}V303R}$ mice (homozygous) displayed normal behavior, grooming, and showed no overt signs of stress, but homozygous mice were noticeably

smaller than littermate hemizygous mice (Fig. 4B). Weights of *Polb*$^{L301R\text{-}V303R/L301R\text{-}V303R}$ mice (homozygous) were significantly smaller (15%) at 17 weeks of age in comparison to *Polb*$^{WT/L301R\text{-}V303R}$ mice (hemizygous) (Fig. 4C). *Polb*$^{L301R\text{-}V303R/L301R\text{-}V303R}$ mice (homozygous) were found to be fertile, with at least three breeding pairs demonstrating nearly equal male and female offspring (Fig. 4D). At present, both male and female *Polb*$^{L301R\text{-}V303R/L301R\text{-}V303R}$ mice (homozygous) have survived for at least 10 months and appear in good health.

3.4 Polb$^{L301R\text{-}V303R/L301R\text{-}V303R}$ cells demonstrate decreased Polβ protein abundance

We have previously shown that disruption of the Polβ/XRCC1 interaction alters Polβ protein stability in human cells [17], so we investigated if this instability was evident in cells from the *Polb*$^{L301R\text{-}V303R/L301R\text{-}V303R}$ mice. We generated SV40 T-antigen immortalized fibroblast cell lines from ear clips of littermate *Polb* WT and *Polb*$^{L301R\text{-}V303R/L301R\text{-}V303R}$ mice. Immunoblotting revealed that Polβ protein abundance was diminished in the *Polb*$^{L301R\text{-}V303R/L301R\text{-}V303R}$ ear fibroblasts compared to WT fibroblasts (Fig. 5A). Using two Polβ antibodies, we observed an 85.5% decrease in Polβ protein abundance (18% remaining with ab26343, 11% with Clone 61, each from single blot images). No change was observed in XRCC1 protein abundance, consistent with previous results [17].

We previously observed that alterations in Polβ protein abundance caused by altered XRCC1 binding did not lead to changes in DNA damage response following genotoxic stress, but these models relied on Polβ overexpression in human cells [17]. To determine if alterations in Polβ's XRCC1 binding capability would affect cell sensitivity to genotoxic stress at endogenous protein levels, we treated *Polb* WT and *Polb*$^{L301R\text{-}V303R/L301R\text{-}V303R}$ fibroblasts with H_2O_2 or MMS and assessed cell survival after 5 days. We did not observe a change in sensitivity for *Polb*$^{L301R\text{-}V303R/L301R\text{-}V303R}$ ear fibroblasts in comparison to WT cells following exposure to either H_2O_2 (Fig. 5B) or MMS (Fig. 5C), confirming our previous results in human cells [17].

4. Discussion

Owing to the critical role of Polβ during BER, understanding the functional impact of Polβ disruption can provide insights into its role in response to endogenous DNA damage and the impact on aging and cancer. We have shown that the recruitment of Polβ to sites of DNA damage is facilitated through its interaction with XRCC1, and the loss of XRCC1 or disruption of Polβ's XRCC1 binding domain are able to prevent detectable Polβ recruitment [12]. We also found that the stability of Polβ is impacted by the disruption of its interaction with XRCC1 [17], but several questions remained to be addressed following these results. Since our previous results relied on protein overexpression in cell line models, the impact of disrupting the Polβ/XRCC1 complex at the endogenous protein level as well as at a higher organismal level could not be appropriately assessed, thereby providing the impetus for our current studies. Here, we generated a mouse model with a CRISPR/Cas9-targeted mutation of Polβ's XRCC1 binding domain (Fig. 4A).

Previous results relied on human and rat Polβ to characterize the interaction domain with XRCC1 [22, 31, 35, 36], so we first validated key amino acid residues responsible for

the interaction between mouse Polβ and XRCC1. We previously used a triple mutant of Polβ with mutations in amino acid residues L301, V303, and V306 that disrupted the interaction between human Polβ and XRCC1 in human cells [17]. These residues are evolutionarily conserved between rat, mouse, and human species (Figs. 1A and S1A). While mutation of V303 (V303R) accounted for a 90.8% reduction in Polβ recruitment to sites of laser-induced DNA damage, the dual mutant L301R/V303R reduced Polβ recruitment to a similar degree as the Polβ L301R/V303R/V306R triple mutant we previously characterized (Figs. 1B,D). While it may be possible, however, unlikely, that the dual mutant of Polβ (L301R/V303R) may recruit very fast and then release from the site of DNA damage within a few seconds, both our previous studies [12] and reports from others [37] argue against such a scenario. In that earlier report from the Wilson group, they investigated laser-induced DNA damage conditions that can be optimized for PARP1-independent (and hence XRCC1-independent) recruitment of Polβ, for example using laser treatment approaches that will induce a significant amount of DNA double-strand breaks, such as the addition of BrdU [37]. Note however, that the laser conditions we use do not promote the recruitment of DNA double-strand break repair proteins [12]. In our work and in the report from the Wilson group, the recruitment peaks range from 45–60s, which does not support the suggestion that the mutant (L301R/V303R) is binding and releasing from the DNA damage site rapidly and hence is undetected. The importance of the V303 residue in mediating an interaction with XRCC1 is further underscored by our structural data (Fig. 3) where *in silico* mutation of this residue to arginine in the rat Polβ structure results in a direct clash with the oxidized form of XRCC1.

Germ-line deletion (knockout, KO) of the mouse *Polb* gene gives rise to perinatal lethality [11]. To overcome the potential developmental detriment to the loss of *Polb*, Rajewsky and colleagues employed the Cre-Lox system to develop a method for conditional gene deletion. In this case, the *Polb* gene was deleted only in T-cells [11]. In this initial conditional KO model, as much as 40% of the T-cells showed complete loss of *Polb*. However, any role for Polβ in T-cell receptor gene rearrangement was not clarified [11]. The Cre-Lox approach was next used to develop mosaic *Polb-KO* mice, further demonstrating the requirement for *Polb* in many tissue types [38]. Since *Polb-KO* mice die essentially at birth (perinatal), *Polb-KO* fetal liver cells were then used to reconstitute lethally irradiated mice to test a role for Polβ in T-cell dependent immunity [9]. However, no role for Polβ was identified in these studies with regard to an immune response [9]. Conditional gene targeting was also used to reveal a role for Polβ in meiotic synapsis [39] and in sperm mutagenesis [40]. It was subsequently determined that Polβ may play a role in neurogenesis [8] that is dependent on p53 [41]. However, a complete mutant animal model was still elusive.

Several mouse models were then developed that express active site mutants or over-express the wild-type protein. These include a mutation in the polymerase domain (Y265C), where most die within a few hours after birth [42], but was eventually shown to be associated with the onset of lupus [43] by a glycosylase dependent mechanism [44]. A mouse with the R137Q mutation was found to be inviable [45] and more recently the L22P mutant mouse was developed that lacks dRP lyase activity [46]. Although the full details of the L22P mouse have not yet been reported, it was suggested that there is enhanced genome instability in response to *H. pylori* infection [46]. Finally, over-expression of wild-type Polβ

led to spontaneous cataracts [47] and an increase in tumor burden [48], highlighting the requirement for balance in the BER pathway [7].

Here, *Polb*$^{L301R\text{-}V303R/L301R\text{-}V303R}$ mice were successfully bred to homozygosity, which stood in contrast to the unsuccessful attempts to generate a homozygous *Polb* knockout mouse [11]. These results suggest that loss of the Polβ/XRCC1 interaction was not the source of the perinatal lethality previously observed. *Polb*$^{L301R\text{-}V303R/L301R\text{-}V303R}$ mice also appeared phenotypically normal except for a decreased size as compared to WT and heterozygous mice (Figs. 4B,C). The 15% decrease in size is not associated with visible physical, motor, or grooming deficiencies nor other outward signs of stress, up to 10 months of age. Longer duration studies will be required to determine if an accelerated aging phenotype or tissue-specific dysfunction becomes apparent as *Polb*$^{L301R\text{-}V303R/L301R\text{-}V303R}$ mice enter later life. We also successfully bred *Polb*$^{L301R\text{-}V303R/L301R\text{-}V303R}$ male and female mice, suggesting that neither male nor female fertility was impacted by disruption of the Polβ/XRCC1 interaction (Fig. 4D). There was no observable difference in the number or gender distribution of offspring from three independent homozygous breeding pairs. These results confirm that Polβ's interaction with XRCC1 is not required for fertility or development. The *Polβ*$^{L301R\text{-}V303R/L301R\text{-}V303R}$ mouse, when challenged with environmental genotoxins or with chemotherapeutic compounds, may demonstrate additional characteristics such as neuronal abnormalities or the onset of a cancer phenotype, but it is too early to assess or hypothesize as of yet as to whether this with be a cancer relevant mouse model. Other reports have suggested that loss of *Polb* may yield a defect in triplet-repeat expansion and stability [49–51] as well as Alzheimer's disease [52, 53] that we will also consider in the future with this model.

Fibroblasts generated from ear clippings of *Polb*$^{L301R\text{-}V303R/L301R\text{-}V303R}$ mice demonstrated that disruption of Polβ's binding to XRCC1 decreased Polβ protein abundance and/or stability (Fig. 5A), which agrees with our previous results from human cell studies [17]. *Polb*$^{L301R\text{-}V303R/L301R\text{-}V303R}$ derived fibroblasts exhibited only 15% Polβ protein abundance as compared to WT mouse fibroblasts, suggesting maintenance of mouse Polβ protein levels is facilitated by its interaction with XRCC1, as seen in human cells [17, 23]. Interestingly, we observed no significant change in sensitivity to genotoxins known to produce BER-associated DNA damage (Figs. 5B,C), which confirmed our previous results obtained in human cell line models. This is also consistent with earlier reports that the oxidized form of XRCC1 plays the major role in binding to Polβ at sites of DNA damage [54] but there is evidence for Polβ dependent response to genotoxins, with regard to survival, that is independent of XRCC1 [55] and the reduced form of XRCC1 shows suppressed levels of Polβ recruitment [56]. These results suggest that the remaining 15% of Polβ protein in the *Polb*$^{L301R\text{-}V303R/L301R\text{-}V303R}$ derived fibroblasts is sufficient to repair and respond to the acute genotoxic stress induced by H_2O_2 and MMS.

Even though the Polβ/XRCC1 binding interface is highly conserved, implying an important role, our data suggest that the interaction between the two proteins is expendable for animal viability, fertility, and development. This leaves us questioning the critical role that this interaction serves, if not facilitating DNA repair. There are numerous possible explanations; the primary one being that disruption of the Polβ/XRCC1 interaction is not critical for

fibroblast cell line DNA repair (i.e., the mouse cell lines used for Fig. 5) but may serve a cell-type-specific function whose impact is not readily apparent in young mice. Previously generated *Polb-KO* mice displayed perinatal lethality associated with aberrant neurogenesis [8], which may suggest enhanced neuronal sensitivity in $Polb^{L301R\text{-}V303R/L301R\text{-}V303R}$ mice. We did not observe any overt motor or behavioral problems in these mice, but this may become more apparent as the mice age or with more sensitive neurological and neuromotor monitoring. However, the importance of the interaction of Polβ with XRCC1, while evident, is not fully characterized, highlighting that more studies would be required to fully elucidate the significance of this interaction.

5. Conclusions

The interaction between Polβ and XRCC1 is primarily mediated by amino acid residue V303, though mutations in L301 and V306 can further weaken this interaction. Structural studies via X-ray crystallography of mouse WT Polβ and L301R/V303R mutant Polβ further confirm the importance of amino acid residue V303 in facilitating an interaction with XRCC1 in a redox-sensitive manner. CRISPR/Cas9-modified $Polb^{L301R\text{-}V303R/L301R\text{-}V303R}$ mice exhibit reduced size as compared to heterozygous mice, but are viable, unlike *Polb-KO* mice. $Polb^{L301R\text{-}V303R/L301R\text{-}V303R}$ mice are fertile, with no gender bias in the offspring and no obvious developmental defects. $Polb^{L301R\text{-}V303R/L301R\text{-}V303R}$ mouse ear fibroblasts demonstrate that loss of the interaction between mouse Polβ and XRCC1 leads to an ~85% decrease in Polβ protein levels but the remaining Polβ protein is likely sufficient for the cellular response to acute genotoxic stress.

Supplementary Material

Refer to Web version on PubMed Central for supplementary material.

Acknowledgements

We would like to thank the University of Alabama Birmingham TGEM core for help in design and creation of the $Polb^{L301R/V303R}$ mouse line. We would also like to thank Alison Beiser for administrative, technical, and material support. We would like to thank Dr. Matthew Benning (Bruker) for his assistance and support during the collection and processing of the crystallographic data.

Funding

Research in the Sobol lab on DNA repair, the analysis of DNA damage and the impact of genotoxic exposure is funded by grants from the NIH [ES029518, CA148629, ES014811, ES028949, CA238061, CA236911, AG069740 and ES032522], from the NSF [NSF-1841811] and a grant from the DOD [GRANT11998991, DURIP-Navy]. Support is also provided by grants from the Breast Cancer Research Foundation of Alabama, from the Abraham A. Mitchell Distinguished Investigator Fund, from the Mitchell Cancer Institute Molecular & Metabolic Oncology Program Development fund and from the Legoretta Cancer Center Endowment Fund (to RWS).

MKT, NS, and AP were supported in part by a grant from the National Institutes of Environmental Health Sciences (NIEHS), Outstanding New Environmental Scientist (ONES) R01 grant #R01ES030084 to AP, and AP is also supported by an NIEHS R35 subcontract grant #R35ES031708 to Dr. Joann Sweasy (University of Arizona). Startup funds provided to AP by the University of South Alabama Health Mitchell Cancer Institute are also acknowledged.

References

[1]. Lindahl T, Instability and decay of the primary structure of DNA, Nature, 362 (1993) 709–715. [PubMed: 8469282]

[2]. Friedberg EC, Walker GC, Siede W, Wood RD, Schultz RA, Ellenberger T, DNA Repair and Mutagenesis, 2nd Edition, ASM Press, Washington, D.C., 2006.

[3]. Svilar D, Goellner EM, Almeida KH, Sobol RW, Base excision repair and lesion-dependent subpathways for repair of oxidative DNA damage, Antioxid Redox Signal, 14 (2011) 2491–2507. [PubMed: 20649466]

[4]. Abbotts R, Wilson DM 3rd, Coordination of DNA single strand break repair, Free Radic Biol Med, 107 (2017) 228–244. [PubMed: 27890643]

[5]. Tang JB, Goellner EM, Wang XH, Trivedi RN, St Croix CM, Jelezcova E, Svilar D, Brown AR, Sobol RW, Bioenergetic metabolites regulate base excision repair-dependent cell death in response to DNA damage, Mol Cancer Res, 8 (2010) 67–79. [PubMed: 20068071]

[6]. Wallace SS, Murphy DL, Sweasy JB, Base excision repair and cancer, Cancer Lett, 327 (2012) 73–89. [PubMed: 22252118]

[7]. Almeida KH, Sobol RW, A unified view of base excision repair: lesion-dependent protein complexes regulated by post-translational modification, DNA Repair (Amst), 6 (2007) 695–711. [PubMed: 17337257]

[8]. Sugo N, Aratani Y, Nagashima Y, Kubota Y, Koyama H, Neonatal lethality with abnormal neurogenesis in mice deficient in DNA polymerase beta, EMBO J, 19 (2000) 1397–1404. [PubMed: 10716939]

[9]. Esposito G, Texido G, Betz UA, Gu H, Muller W, Klein U, Rajewsky K, Mice reconstituted with DNA polymerase beta-deficient fetal liver cells are able to mount a T cell-dependent immune response and mutate their Ig genes normally, Proc Natl Acad Sci U S A, 97 (2000) 1166–1171. [PubMed: 10655502]

[10]. Sobol RW, Horton JK, Kuhn R, Gu H, Singhal RK, Prasad R, Rajewsky K, Wilson SH, Requirement of mammalian DNA polymerase-beta in base-excision repair, Nature, 379 (1996) 183–186. [PubMed: 8538772]

[11]. Gu H, Marth JD, Orban PC, Mossmann H, Rajewsky K, Deletion of a DNA polymerase beta gene segment in T cells using cell type-specific gene targeting, Science, 265 (1994) 103–106. [PubMed: 8016642]

[12]. Koczor CA, Saville KM, Andrews JF, Clark J, Fang Q, Li J, Al-Rahahleh RQ, Ibrahim M, McClellan S, Makarov MV, Migaud ME, Sobol RW, Temporal dynamics of base excision/single-strand break repair protein complex assembly/disassembly are modulated by the PARP/NAD(+)/SIRT6 axis, Cell reports, 37 (2021) 109917.

[13]. Almeida KH, Sobol RW, Increased Specificity and Efficiency of Base Excision Repair through Complex Formation, in: Siede W, Doetsch PW, Kow YW (Eds.) DNA Damage Recognition, Marcel Dekker Inc., New York, 2005, pp. 33–64.

[14]. Ray Chaudhuri A, Nussenzweig A, The multifaceted roles of PARP1 in DNA repair and chromatin remodelling, Nat Rev Mol Cell Biol, 18 (2017) 610–621. [PubMed: 28676700]

[15]. El-Khamisy SF, Masutani M, Suzuki H, Caldecott KW, A requirement for PARP-1 for the assembly or stability of XRCC1 nuclear foci at sites of oxidative DNA damage, Nucleic Acids Res, 31 (2003) 5526–5533. [PubMed: 14500814]

[16]. Breslin C, Hornyak P, Ridley A, Rulten SL, Hanzlikova H, Oliver AW, Caldecott KW, The XRCC1 phosphate-binding pocket binds poly (ADP-ribose) and is required for XRCC1 function, Nucleic Acids Res, 43 (2015) 6934–6944. [PubMed: 26130715]

[17]. Fang Q, Inanc B, Schamus S, Wang XH, Wei L, Brown AR, Svilar D, Sugrue KF, Goellner EM, Zeng X, Yates NA, Lan L, Vens C, Sobol RW, HSP90 regulates DNA repair via the interaction between XRCC1 and DNA polymerase beta, Nature communications, 5 (2014) 5513.

[18]. Whitaker AM, Freudenthal BD, History of DNA polymerase beta X-ray crystallography, DNA Repair (Amst), 93 (2020) 102928.

[19]. Shock DD, Freudenthal BD, Beard WA, Wilson SH, Modulating the DNA polymerase beta reaction equilibrium to dissect the reverse reaction, Nat Chem Biol, 13 (2017) 1074–1080. [PubMed: 28759020]

[20]. Batra VK, Beard WA, Pedersen LC, Wilson SH, Structures of DNA Polymerase Mispaired DNA Termini Transitioning to Pre-catalytic Complexes Support an Induced-Fit Fidelity Mechanism, Structure, 24 (2016) 1863–1875. [PubMed: 27642161]

[21]. Sawaya MR, Prasad R, Wilson SH, Kraut J, Pelletier H, Crystal structures of human DNA polymerase beta complexed with gapped and nicked DNA: evidence for an induced fit mechanism, Biochemistry, 36 (1997) 11205–11215. [PubMed: 9287163]

[22]. Cuneo MJ, London RE, Oxidation state of the XRCC1 N-terminal domain regulates DNA polymerase beta binding affinity, Proc Natl Acad Sci U S A, 107 (2010) 6805–6810. [PubMed: 20351257]

[23]. Fang Q, Andrews J, Sharma N, Wilk A, Clark J, Slyskova J, Koczor CA, Lans H, Prakash A, Sobol RW, Stability and sub-cellular localization of DNA polymerase beta is regulated by interactions with NQO1 and XRCC1 in response to oxidative stress, Nucleic Acids Res, 47 (2019) 6269–6286. [PubMed: 31287140]

[24]. Sobol RW, Kartalou M, Almeida KH, Joyce DF, Engelward BP, Horton JK, Prasad R, Samson LD, Wilson SH, Base excision repair intermediates induce p53-independent cytotoxic and genotoxic responses, J Biol Chem, 278 (2003) 39951–39959. [PubMed: 12882965]

[25]. Khan M, Gasser S, Generating Primary Fibroblast Cultures from Mouse Ear and Tail Tissues, Journal of visualized experiments : JoVE, (2016).

[26]. Fouquerel E, Goellner EM, Yu Z, Gagne JP, Barbi de Moura M, Feinstein T, Wheeler D, Redpath P, Li J, Romero G, Migaud M, Van Houten B, Poirier GG, Sobol RW, ARTD1/PARP1 negatively regulates glycolysis by inhibiting hexokinase 1 independent of NAD+ depletion, Cell reports, 8 (2014) 1819–1831. [PubMed: 25220464]

[27]. McCoy AJ, Grosse-Kunstleve RW, Adams PD, Winn MD, Storoni LC, Read RJ, Phaser crystallographic software J Appl Crystallogr, 40 (2007) 658–674.

[28]. Adams PD, Afonine PV, Bunkoczi G, Chen VB, Davis IW, Echols N, Headd JJ, Hung LW, Kapral GJ, Grosse-Kunstleve RW, McCoy AJ, Moriarty NW, Oeffner R, Read RJ, Richardson DC, Richardson JS, Terwilliger TC, Zwart PH, PHENIX: a comprehensive Python-based system for macromolecular structure solution, Acta Crystallogr D Biol Crystallogr, 66 (2010) 213–221. [PubMed: 20124702]

[29]. Emsley P, Lohkamp B, Scott WG, Cowtan K, Features and development of Coot, Acta Crystallogr D Biol Crystallogr, 66 (2010) 486–501. [PubMed: 20383002]

[30]. Williams CJ, Headd JJ, Moriarty NW, Prisant MG, Videau LL, Deis LN, Verma V, Keedy DA, Hintze BJ, Chen VB, Jain S, Lewis SM, Arendall WB 3rd, Snoeyink J, Adams PD, Lovell SC, Richardson JS, Richardson DC, MolProbity: More and better reference data for improved all-atom structure validation, Protein Sci, 27 (2018) 293–315. [PubMed: 29067766]

[31]. Marintchev A, Robertson A, Dimitriadis EK, Prasad R, Wilson SH, Mullen GP, Domain specific interaction in the XRCC1-DNA polymerase beta complex, Nucleic Acids Res, 28 (2000) 2049–2059. [PubMed: 10773072]

[32]. Davies JF, 2nd, R.J. Almassy, Z. Hostomska, R.A. Ferre, Z. Hostomsky, 2.3 A crystal structure of the catalytic domain of DNA polymerase beta, Cell, 76 (1994) 1123–1133. [PubMed: 8137427]

[33]. Pelletier H, Sawaya MR, Characterization of the metal ion binding helix-hairpin-helix motifs in human DNA polymerase beta by X-ray structural analysis, Biochemistry, 35 (1996) 12778–12787. [PubMed: 8841120]

[34]. Liptak C, Mahmoud MM, Eckenroth BE, Moreno MV, East K, Alnajjar KS, Huang J, Towle-Weicksel JB, Doublie S, Loria JP, Sweasy JB, I260Q DNA polymerase beta highlights precatalytic conformational rearrangements critical for fidelity, Nucleic Acids Res, 46 (2018) 10740–10756. [PubMed: 30239932]

[35]. Marintchev A, Mullen MA, Maciejewski MW, Pan B, Gryk MR, Mullen GP, Solution structure of the single-strand break repair protein XRCC1 N-terminal domain, Nat Struct Biol, 6 (1999) 884–893. [PubMed: 10467102]

[36]. Marintchev A, Gryk MR, Mullen GP, Site-directed mutagenesis analysis of the structural interaction of the single-strand-break repair protein, X-ray cross-complementing group 1, with DNA polymerase beta, Nucleic Acids Res, 31 (2003) 580–588. [PubMed: 12527765]

[37]. Howard MJ, Horton JK, Zhao ML, Wilson SH, Lysines in the lyase active site of DNA polymerase beta destabilize nonspecific DNA binding, facilitating searching and DNA gap recognition, J Biol Chem, 295 (2020) 12181–12187. [PubMed: 32647014]

[38]. Betz UA, Vosshenrich CA, Rajewsky K, Muller W, Bypass of lethality with mosaic mice generated by Cre-loxP-mediated recombination, Curr Biol, 6 (1996) 1307–1316. [PubMed: 8939573]

[39]. Kidane D, Jonason AS, Gorton TS, Mihaylov I, Pan J, Keeney S, de Rooij DG, Ashley T, Keh A, Liu Y, Banerjee U, Zelterman D, Sweasy JB, DNA polymerase beta is critical for mouse meiotic synapsis, EMBO J, 29 (2010) 410–423. [PubMed: 20019666]

[40]. Kidane D, Dalal S, Keh A, Liu Y, Zelterman D, Sweasy JB, DNA polymerase beta is critical for genomic stability of sperm cells, DNA Repair (Amst), 10 (2011) 390–397. [PubMed: 21333614]

[41]. Sugo N, Niimi N, Aratani Y, Takiguchi-Hayashi K, Koyama H, p53 Deficiency rescues neuronal apoptosis but not differentiation in DNA polymerase beta-deficient mice, Mol Cell Biol, 24 (2004) 9470–9477. [PubMed: 15485914]

[42]. Senejani AG, Dalal S, Liu Y, Nottoli TP, McGrath JM, Clairmont CS, Sweasy JB, Y265C DNA polymerase beta knockin mice survive past birth and accumulate base excision repair intermediate substrates, Proc Natl Acad Sci U S A, 109 (2012) 6632–6637. [PubMed: 22493258]

[43]. Senejani AG, Liu Y, Kidane D, Maher SE, Zeiss CJ, Park HJ, Kashgarian M, McNiff JM, Zelterman D, Bothwell AL, Sweasy JB, Mutation of POLB causes lupus in mice, Cell reports, 6 (2014) 1–8. [PubMed: 24388753]

[44]. Paluri SL, Burak M, Senejani AG, Levinson M, Rahim T, Clairmont K, Kashgarian M, Alvarado-Cruz I, Meas R, Cardo-Vila M, Zeiss C, Maher S, Bothwell ALM, Coskun E, Kant M, Jaruga P, Dizdaroglu M, Stephen Lloyd R, Sweasy JB, DNA glycosylase deficiency leads to decreased severity of lupus in the Polb-Y265C mouse model, DNA Repair (Amst), 105 (2021) 103152.

[45]. Pan F, Zhao J, Zhou T, Kuang Z, Dai H, Wu H, Sun H, Zhou X, Wu X, Hu Z, He L, Shen B, Guo Z, Mutation of DNA Polymerase beta R137Q Results in Retarded Embryo Development Due to Impaired DNA Base Excision Repair in Mice, Sci Rep, 6 (2016) 28614. [PubMed: 27358192]

[46]. Zhao S, Thakur M, Klattenhoff AW, Kidane D, Aberrant DNA Polymerase Beta Enhances H. pylori Infection Induced Genomic Instability and Gastric Carcinogenesis in Mice, Cancers (Basel), 11 (2019).

[47]. Sobol RW, Foley JF, Nyska A, Davidson MG, Wilson SH, Regulated over-expression of DNA polymerase beta mediates early onset cataract in mice, DNA Repair (Amst), 2 (2003) 609–622. [PubMed: 12713817]

[48]. Yoshizawa K, Jelezcova E, Brown AR, Foley JF, Nyska A, Cui X, Hofseth LJ, Maronpot RM, Wilson SH, Sepulveda AR, Sobol RW, Gastrointestinal hyperplasia with altered expression of DNA polymerase beta, PLoS ONE, 4 (2009) e6493. [PubMed: 19654874]

[49]. Lokanga RA, Senejani AG, Sweasy JB, Usdin K, Heterozygosity for a hypomorphic Polbeta mutation reduces the expansion frequency in a mouse model of the Fragile X-related disorders, PLoS Genet, 11 (2015) e1005181.

[50]. Crespan E, Hubscher U, Maga G, Expansion of CAG triplet repeats by human DNA polymerases lambda and beta in vitro, is regulated by flap endonuclease 1 and DNA ligase 1, DNA Repair (Amst), 29 (2015) 101–111. [PubMed: 25687118]

[51]. Xu M, Gabison J, Liu Y, Trinucleotide repeat deletion via a unique hairpin bypass by DNA polymerase beta and alternate flap cleavage by flap endonuclease 1, Nucleic Acids Res, 41 (2013) 1684–1697. [PubMed: 23258707]

[52]. Misiak M, Vergara Greeno R, Baptiste BA, Sykora P, Liu D, Cordonnier S, Fang EF, Croteau DL, Mattson MP, Bohr VA, DNA polymerase beta decrement triggers death of olfactory bulb cells and impairs olfaction in a mouse model of Alzheimer's disease, Aging Cell, 16 (2017) 162–172. [PubMed: 27686631]

[53]. Sykora P, Misiak M, Wang Y, Ghosh S, Leandro GS, Liu D, Tian J, Baptiste BA, Cong WN, Brenerman BM, Fang E, Becker KG, Hamilton RJ, Chigurupati S, Zhang Y, Egan JM,

Croteau DL, Wilson DM 3rd, Mattson MP, Bohr VA, DNA polymerase beta deficiency leads to neurodegeneration and exacerbates Alzheimer disease phenotypes, Nucleic Acids Res, 43 (2015) 943–959. [PubMed: 25552414]

[54]. Horton JK, Stefanick DF, Gassman NR, Williams JG, Gabel SA, Cuneo MJ, Prasad R, Kedar PS, Derose EF, Hou EW, London RE, Wilson SH, Preventing oxidation of cellular XRCC1 affects PARP-mediated DNA damage responses, DNA Repair (Amst), 12 (2013) 774–785. [PubMed: 23871146]

[55]. Horton JK, Gassman NR, Dunigan BD, Stefanick DF, Wilson SH, DNA polymerase beta-dependent cell survival independent of XRCC1 expression, DNA Repair (Amst), 26 (2015) 23–29. [PubMed: 25541391]

[56]. Horton JK, Seddon HJ, Zhao ML, Gassman NR, Janoshazi AK, Stefanick DF, Wilson SH, Role of the oxidized form of XRCC1 in protection against extreme oxidative stress, Free Radic Biol Med, 107 (2017) 292–300. [PubMed: 28179111]

Highlights

- Mouse Polβ requires XRCC1 binding to recruit to sites of DNA damage.
- Mouse viability is independent of the Polβ/XRCC1 interaction.
- Cellular protein stability of Polβ is, in part, dependent on XRCC1.
- Conformation of mouse Polβ WT vs R301/303 is not significantly different.
- Polβ residue V303 is important for an interaction with oxidized XRCC1.

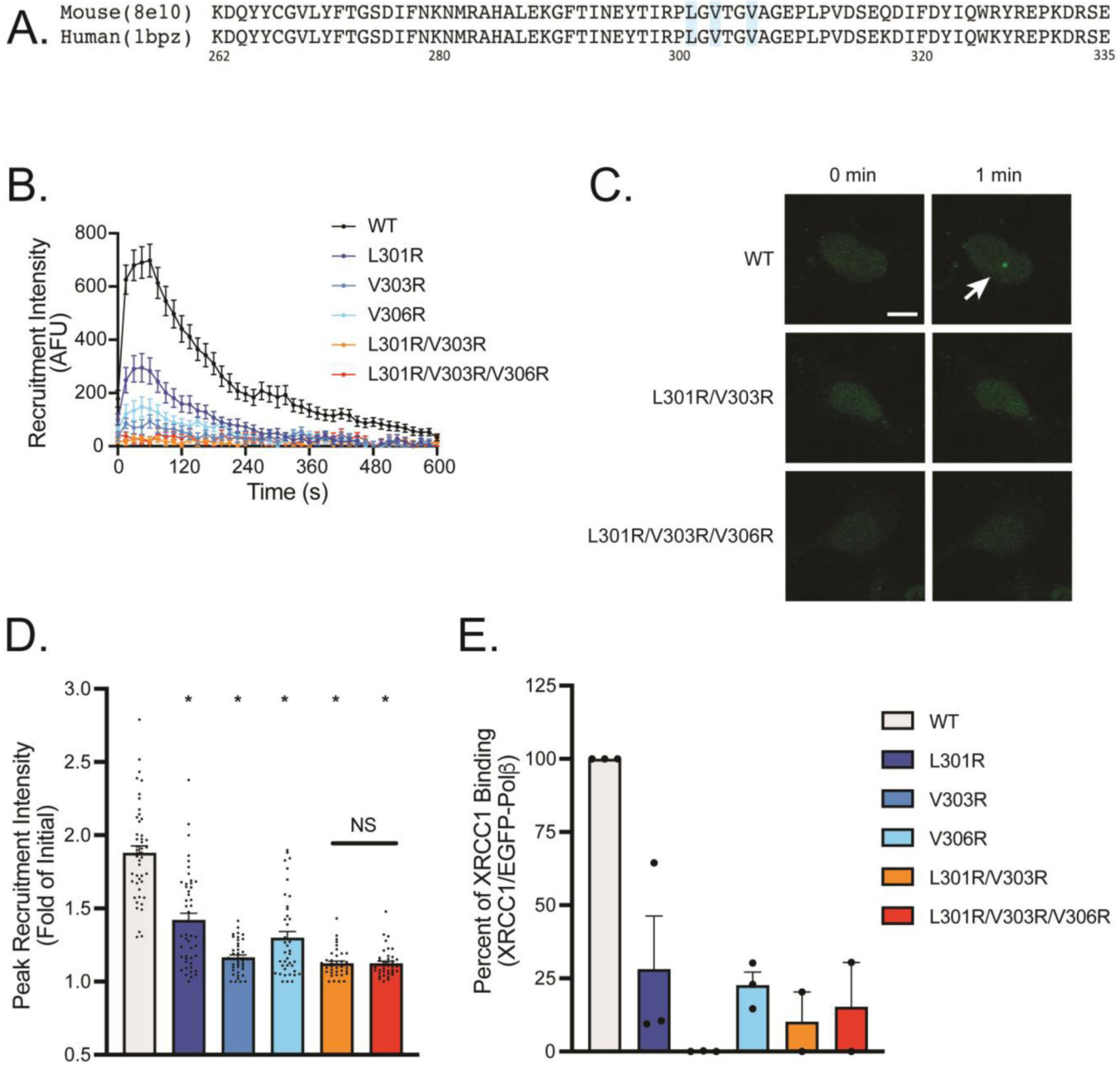

Figure 1: Disruption of Polβ/XRCC1 heterodimerization.

A) Polβ's XRCC1 interaction interface contains the V303 loop with residues L301, V303, and V306 (shaded blue) implicated in facilitating Polβ's interaction with XRCC1; **B)** EGFP-Polβ recruitment profiles following 355nm laser micro-irradiation. Polβ L301R/V303R and Polβ L301/V303R/V306R proteins have no detectable recruitment, N≥40 for each set; **C)** Images of EGFP-Polβ focus formation following laser-induced DNA damage. A visible EGFP-Polβ focus forms 1 min following laser micro-irradiation (white arrow), but EGFP-Polβ L301R/V303R and L301R/V303R/V306R fail to form foci. Extended panels can be found in Fig. S1B. The white scale bar denotes 10μm; **D)** Peak recruitment

intensity of EGFP-Polβ and associated XRCC1-binding mutant proteins. Polβ L301R/V303R and L301R/V303R/V306R demonstrated greater than 95% reduction in peak recruitment and no significant difference from non-micro-irradiated cells, N≥40 for each set; **E)** Immunoprecipitation of XRCC1 using EGFP-Polβ via GFP-Trap demonstrates mutations at L301, V303, and V306 disrupt the Polβ/XRCC1 interaction to varying degrees. Western blots can be found in Fig. S1C, N≥2 for each set.

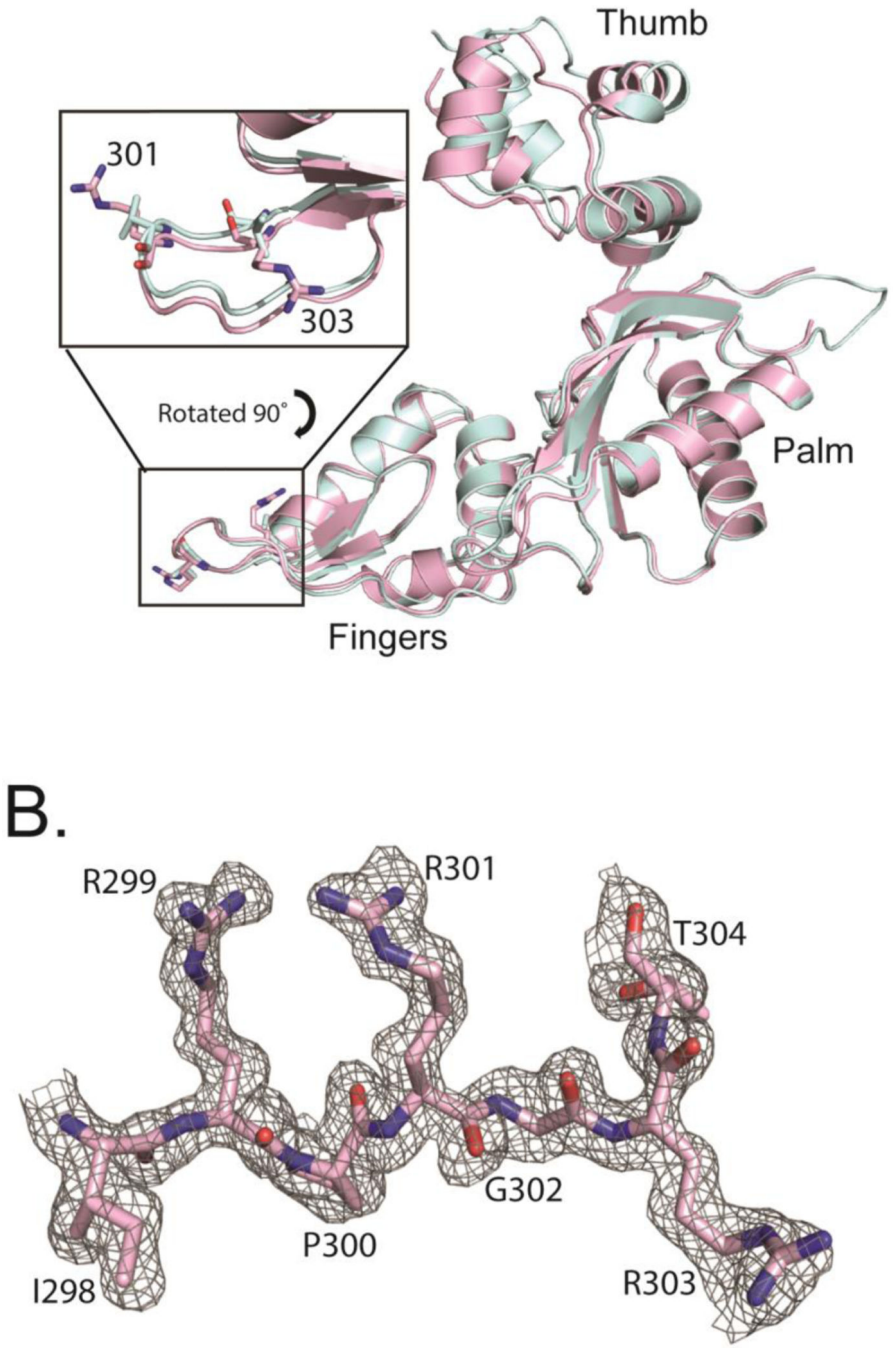

Figure 2: Crystal structures of unliganded mouse WT and mutant Polβ lacking the lyase domain. **A)** Superimposition of WT Polβ (light blue) and mutant Polβ L301R/V303R (light pink). A zoomed in view of the V303 loop, which harbors both arginine mutations, is highlighted in the inset. Overall RMSD of Cα for chain A is 0.536Å, while the RMSD of the Cα of the V303 loop (residues 300–309) is 0.305Å. The RMSD of all backbone atoms for the V303 loop superimposition is 0.314Å; **B)** Simulated annealing composite omit map for residues 298–304 contoured at 1σ displays clear density for two mutated arginine residues, R301 and R303.

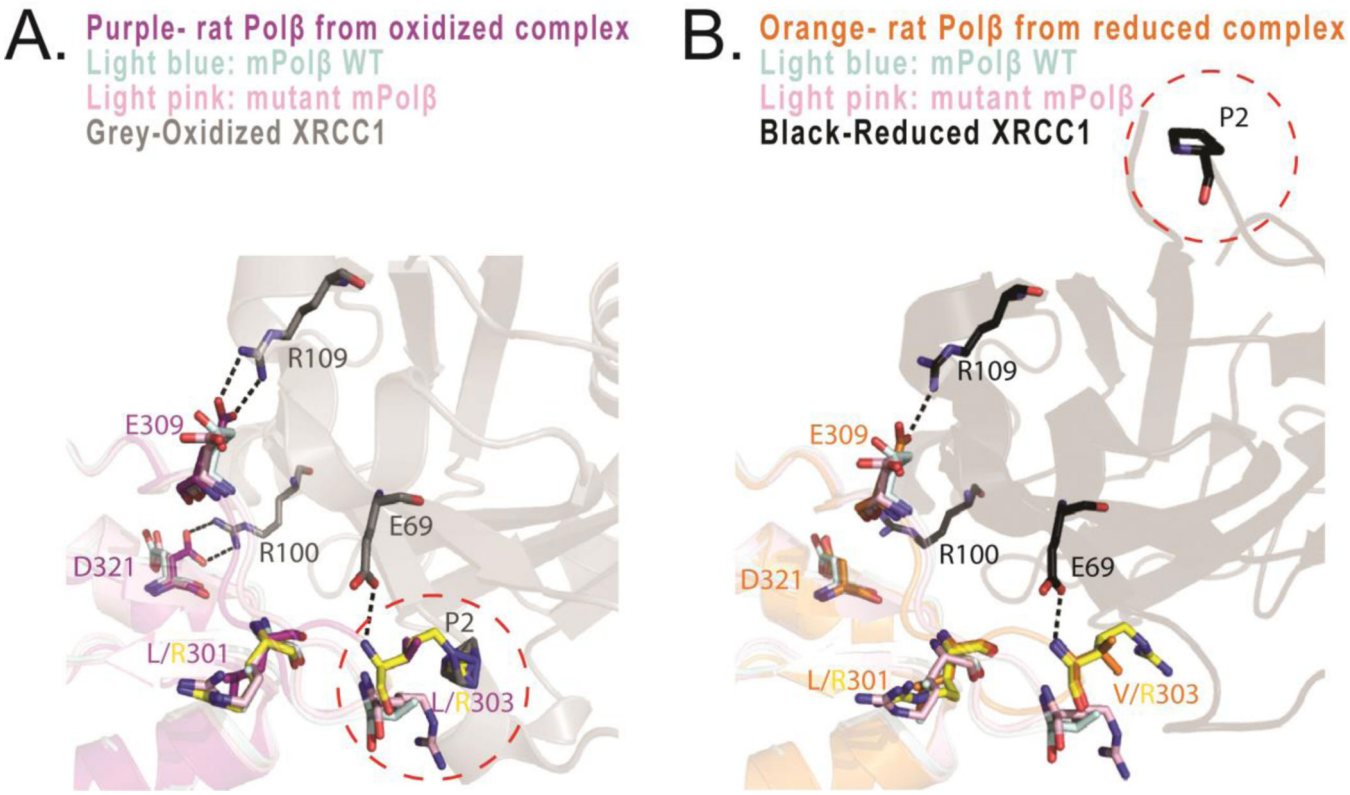

Figure 3: Polβ/XRCC1 interaction interface displaying the L301R/V303R mutations.

A) Interaction interface showing the location of the L301R/V303R mutations compared with rat Polβ interacting with XRCC1 shown in the oxidized form (PDB ID: 3LQC): Light blue: mPolβ WT; Light pink: mPolβ L301R/V303R; Purple: rat Polβ in 3LQC (Polβ bound to oxidized XRCC1) with mutations R301 and R303 manually generated in Coot (yellow sticks); Grey: XRCC1 in 3LQC (Polβ bound to oxidized XRCC1). Black dashes represent interactions between rat Polβ and XRCC1 in 3LQC; **B)** Interaction interface showing the location of the L301R/V303R mutations compared with rat Polβ interacting with XRCC1 shown in the reduced form (PDB ID: 3K75): Light blue: mPolβ WT; Light pink: mPolβ L301R/V303R; Orange: rat Polβ in 3K75 (Polβ bound to reduced XRCC1) with mutations R301 and R303 manually generated in Coot (yellow sticks); Black: XRCC1 in 3K75 (Polβ bound to reduced XRCC1). Black dashes represent interactions between rat Polβ and XRCC1 in 3K75.

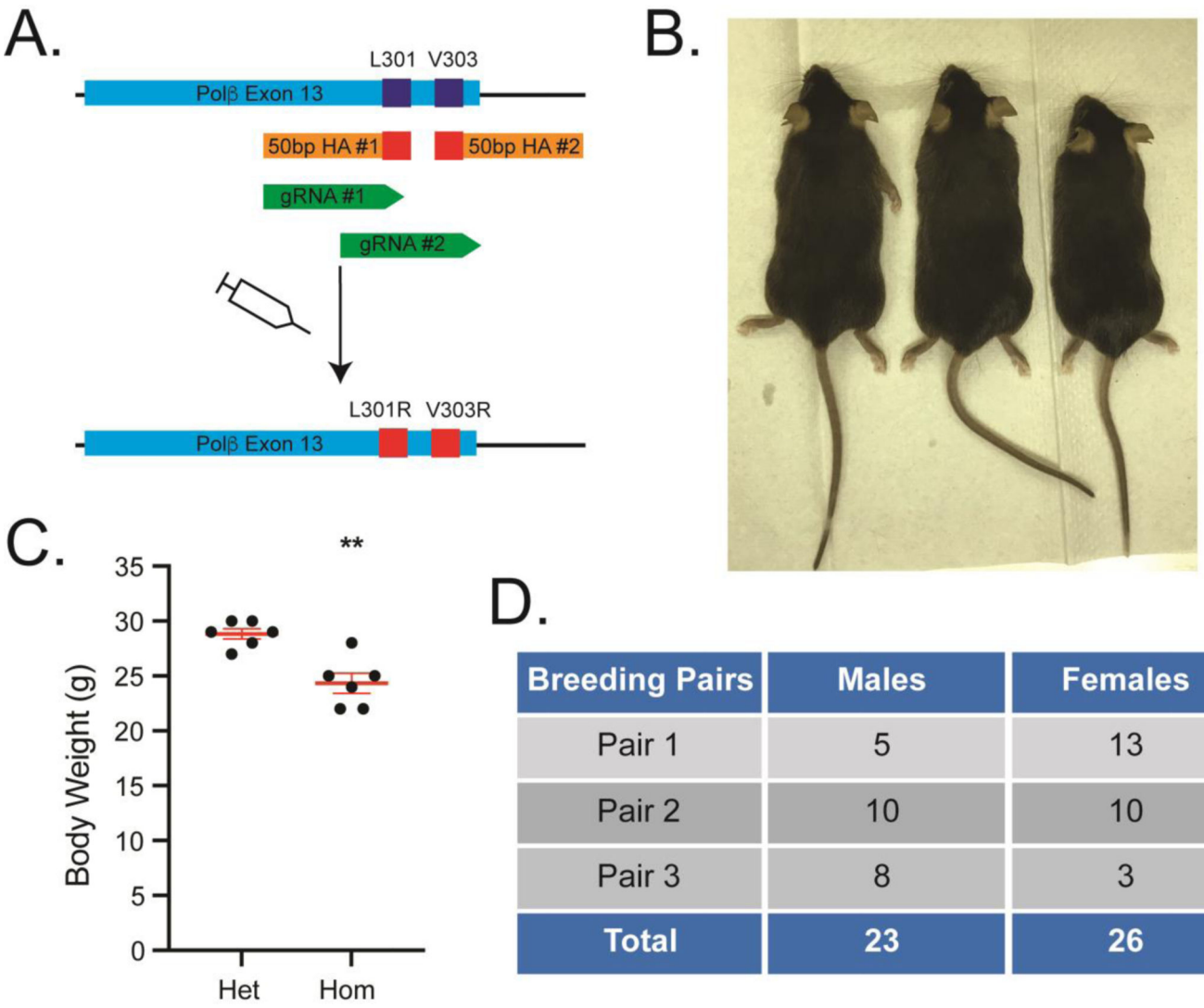

Breeding Pairs	Males	Females
Pair 1	5	13
Pair 2	10	10
Pair 3	8	3
Total	**23**	**26**

Figure 4: *Polb*$^{L301R\text{-}V303R/L301R\text{-}V303R}$ mice are viable and fertile, yet smaller in size.

A) Two gRNAs and two 50bp homologous oligonucleotides were used to target codons corresponding to Polβ amino acid residues L301 and V303. CRISPR/Cas9 complexes were microinjected into 0.5 day old C57Bl/6 mouse embryos and the resulting pups were characterized; **B)** Male littermate C57Bl/6 offspring at 17 weeks of age (L to R): WT, heterozygous *Polb*$^{WT/L301R\text{-}V303R}$, and homozygous *Polb*$^{L301R\text{-}V303R/L301R\text{-}V303R}$; **C)** *Polb*$^{L301R\text{-}V303R/L301R\text{-}V303R}$ mice are significantly smaller in size at 17 weeks in comparison to *Polb*$^{WT/L301R\text{-}V303R}$ mice, N=6 for each set; **D)** *Polb*$^{L301R\text{-}V303R/L301R\text{-}V303R}$ mice are fertile, with no apparent gender bias in offspring. Each breeding pair was independent and had at least 2 litters.

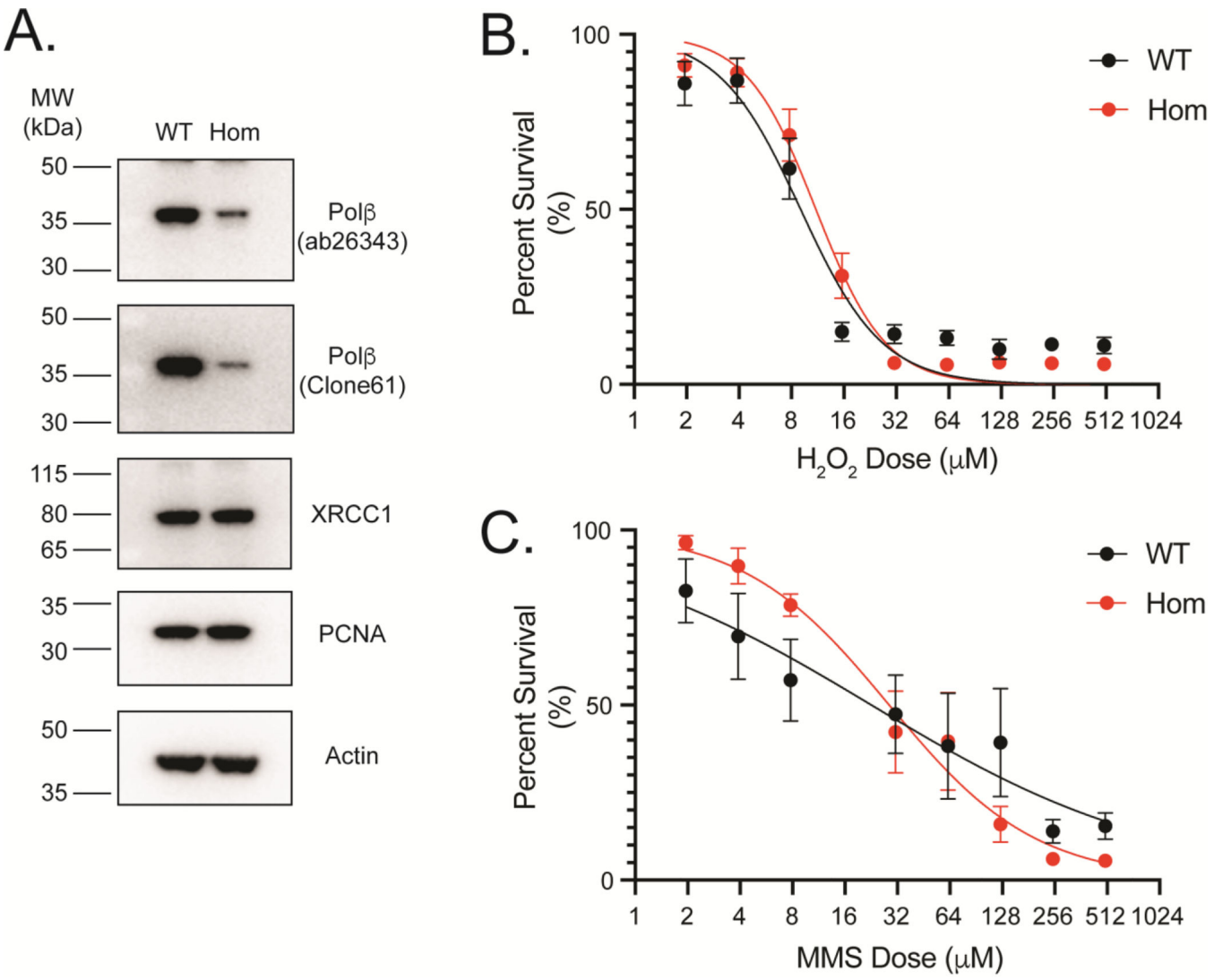

Figure 5: Disrupting Polβ/XRCC1 heterodimerization decreases Polβ protein abundance.

A) Protein isolates from immortalized mouse ear fibroblasts generated from Polβ WT and *Polb*$^{L301R\text{-}V303R/L301R\text{-}V303R}$ C57Bl/6 mice. Two different Polβ antibodies demonstrated that disruption of the Polβ/XRCC1 interaction domain reduced Polβ protein levels in cells by 85%. No change in the expression level of XRCC1 was observed; **B)** Polβ WT and *Polb*$^{L301R\text{-}V303R/L301R\text{-}V303R}$ mouse fibroblasts demonstrated similar sensitivity to H_2O_2 5 days following treatment, N≥3 for each set; **C)** Polβ WT and *Polb*$^{L301R\text{-}V303R/L301R\text{-}V303R}$ mouse fibroblasts demonstrated similar sensitivity to MMS 5 days following treatment, N≥3 for each set.

Table 1.

$Rmerge = \sum \| I - \langle I \rangle \| / \sum I$, where $\langle I \rangle$ is the average intensity from multiple observations of symmetry-related reflections. R_{work} and $R_{free} = \sum \| Fo \| - \| Fc \| / \sum \| Fo \|$, where F_o and F_c are the observed and calculated structure factor amplitudes, respectively. R_{free} was calculated with 10% of the reflections not used in refinement. MR, molecular replacement. Values for the highest resolution shell are shown in parentheses.

	mPolβ WT	**mPolβ L301R V303R**
Beamline	Home source (D8 Quest, Bruker)	Home source (D8 Quest, Bruker)
Wavelength (Å)	1.5418	1.5418
Space group	P 21 21 2	C 1 2 1
Unit-cell parameters (Å,°)	a=62.72, b=120.53, c=69.04	a=160.37, b=39.90, c=93.80,
Molecules per asymmetric unit	α=90, β=90, γ=90 2	α=90, β=91.71, γ=90 2
Data collection statistics		
Resolution range (Å)	34.52–1.65 (1.68–1.65)	31.25–1.80 (1.84–1.80)
Unique reflections	63778 (3092)	55670 (3275)
Redundancy	8.0 (6.3)	7.9 (5.2)
Rmerge	0.077 (0.928)	0.084 (1.088)
Rmeas	0.088 (1.111)	0.090 (1.207)
Rpim	0.043 (0.602)	0.031 (0.515)
CC1/2	0.999 (0.625)	0.999 (0.681)
Overall I/σ	20.4 (1.9)	18.4 (1.8)
Completeness (%)	100.00 (99.9)	100.00 (99.8)
MR phasing statistics		
Top LLG	2449.550	2835.958
Top TFZ	15.8	11.9
Refinement Statistics		
Reflections used in refinement	63708 (6264)	55649 (5484)
Reflections used for R-free	6525 (659)	5656 (549)
R_{work} (%)	0.1734 (0.2305)	0.1923 (0.2648)
R_{free} (%)	0.2142 (0.2805)	0.2308 (0.3028)
CC_{work}	0.968 (0.859)	0.960 (0.857)
CC_{free}	0.949 (0.826)	0.941 (0.796)
Number of non-hydrogen atoms	4550	4336
Macromolecules	3982	3900
Ligands	14	22
Solvent	554	414
r.m.s.d values		
Bond length (Å)	0.011	0.005
Bond angles (°)	1.06	0.72
B-factor (Å^2)		
Wilson B	17.41	17.43
Macromolecules	16.29	21.95

	mPolβ WT	mPolβ L301R V303R
Ligands	27.72	31.07
Water	25.15	25.87
Ramachandran plot		
Ramachandran favored (%)	99.38	99.15
Ramachandran allowed (%)	0.62	0.85
Ramachandran outliers (%)	0.00	0.0
Clashscore	0.76	0.65